Novel Morphological Features for Non-mass-like Breast Lesion Classification on DCE-MRI

Mohammad Razavi[1], Lei Wang[1,5], Tao Tan[2], Nico Karssemeijer[2], Lars Linsen[3], Udo Frese[4], Horst K. Hahn[1], and Gabriel Zachmann[4]

[1] Fraunhofer MEVIS - Institute for Medical Image Computing, Bremen, Germany
[2] Radboud University Medical Center, Nijmegen, The Netherlands
[3] Jacobs University Bremen, Bremen, Germany
[4] University of Bremen, Bremen, Germany
[5] Surpath Medical GmbH, Würzburg, Germany

Abstract. For both visual analysis and computer assisted diagnosis systems in breast MRI reading, the delineation and diagnosis of ductal carcinoma in situ (DCIS) is among the most challenging tasks. Recent studies show that kinetic features derived from dynamic contrast enhanced MRI (DCE-MRI) are less effective in discriminating malignant non-masses against benign ones due to their similar kinetic characteristics. Adding shape descriptors can improve the differentiation accuracy. In this work, we propose a set of novel morphological features using the sphere packing technique, aiming to discriminate non-masses based on their shapes. The feature extraction, selection and the classification modules are integrated into a computer-aided diagnosis (CAD) system. The evaluation was performed on a data set of 106 non-masses extracted from 86 patients, which achieved an accuracy of 90.56%, precision of 90.3%, and area under the receiver operating characteristic (ROC) curve (AUC) of 0.94 for the differentiation of benign and malignant types.

1 Introduction

Dynamic contrast enhanced MRI (DCE-MRI) has been widely used in breast cancer screening of high risk patients, preoperative staging, and post-treatment follow-up, for its high sensitivity. According to the BI-RADS lexicon, based on the morphological characteristics, the lesions are classified into mass-like, non-mass-like, and foci [1]. The diagnosis of breast cancer in its intraductal stage might help to prevent it from becoming invasive cancer [2]. However, the delineation and diagnosis of non-masses, most notably DCIS, is challenging in breast MRI reading even for human observers [2, 3]. Clinical evidences show that the kinetic parameters have the potential to distinguish benign and malignant in masses more effectively, but fail to demonstrate usefulness in discriminating the non-masses [3]. Therefore, the computer-aided diagnosis (CAD) tools strongly relying on kinetic features often fail in classifying non-masses. In terms of sensitivity and specificity in non-masses, no previous trials achieved a performance matching CAD approaches for solid masses [2]. To achieve better performance,

there is a demand for prominent morphological features depicting the lesion shapes and distributions [1].

Recently, a few CAD systems focusing on differentiating non-masses in MRI have been reported [4, 5]. Chen et al. [4] combines the kinetic features derived from characteristic kinetic curves (CKCs), morphological and texture features, which were tested with a collection of both mass and non-mass lesions and yield an AUC of 0.85. Hoffmann et al. [5] evaluated the discriminative power of a set of morphological and kinetic descriptors separately, and the Zernike velocity moments, capturing the joint spatiotemporal behaviors of the lesions, to diagnose a collection of non-mass-like breast lesions. However, none of the features exceeds an AUC value of 0.8. Goto et al. [6] directly compared the diagnostic performance of DCE-MRI (early enhancement) with that of high-spatial-resolution MRI (morphologic features) for the first time. They claimed that in the majority of cases breast lesions were correctly diagnosed merely based on certain morphologic features, which makes those features more important than early enhancement for differentiating malignant breast lesions from benign. The accuracy of 95% and 87% were achieved for masses and non-masses respectively.

In this work, we propose three novel morphological features, describing lesion shapes based on the already existing sphere packing algorithm [7], in combination with Zernike descriptors [8]. These features lead to a more precise shape based delineation of malignant and benign lesions and thus a higher discrimination accuracy. Beside introduction of novel morphological features, the contribution of this paper lies in the feature extraction and selection of the features and the evaluation of their performance in discriminating benign and malignant non-mass-like lesions. All these feature types are integrated as modules into a CAD framework implemented on MeVisLab platform[1]. The processing pipeline depicting each individual module is shown in Fig.1. To test the performance of the introduced features, we conducted several experiments using a data set including 86 patients with 106 non-mass-like lesions, among which 68 were pathologically confirmed malignant, and 38 were benign findings. We evaluated the classifier performance using the mentioned features with a Random Forest (RF) classifier in a 10-fold cross-validation scheme, and we achieved an accuracy of 90.56%, precision of 90.3%, and the area under the ROC curve (AUC) value of 0.94.
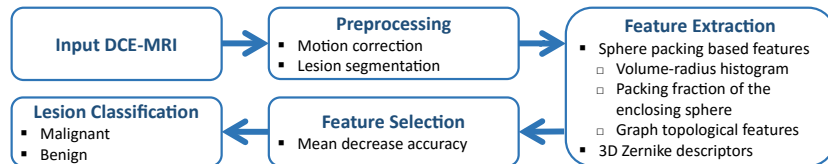
Fig. 1. The integrated framework comprising preprocessing, feature extraction and selection, and lesion analysis modules.

---

[1] MeVisLab: Medical image processing and visualization platform: http://www.mevislab.de [Accessed on 16 March 2016]

2 Materials and Methods

2.1 Imaging Technique and Data Set

The DCE-MRI images were acquired on a 1.5 T scanner (Magnetom Vision, Siemens, Erlangen) in Nijmegen, Netherlands. A dedicated breast coil (CP Breast Array, Siemens, Erlangen) was used in prone patient placement. The pixel spacing differed between volumes with values ranging from 0.625 mm to 0.722 mm. The slice thickness was 1.3 mm, and the volume size was $512 \times 256 \times 120$ voxels. TR and TE were 6.80 s and 4.00 s, respectively, at a 20 degree flip angle. All patients were histologically confirmed by needle aspiration/excision biopsy or surgical removal. Subsequently, the amount of malignant lesions were 68, most of which were diagnosed as DCIS. The rest were diagnosed as invasive ductal carcinoma (IDC), invasive lobular carcinoma (ILC), lobular carcinoma in situ (LCIS) and metastasis. On the other hand, benign histologic findings were found in 38 lesions including fibrocystic changes (FCC), adenosis and hyperplasia. One experienced radiologist retrospectively reviewed the histologic reports and identified the reported lesions. All the lesions were manually segmented with a computer-assistant tool using region-growing and manual correction.

2.2 Feature Extraction

A total of four morphological features are proposed, including three novel shape descriptors based on the already existing data structure generated by sphere packing algorithm, plus the Zernike descriptors. These features are able to efficiently describe the shape and distribution properties of the lesions.

Features based on sphere packing The morphological features that we explored are extracted using the data structures generated by the sphere packing technique [7], which is a new and promising data representation for several fundamental problems in computer graphics and virtual reality, such as collision detection and deformable object simulation. The algorithm iteratively fills the lesion with a fixed number of non-overlapping spheres starting with the one with the largest possible radius, under the condition that they should completely locate inside the lesion. Next, all the components of the spheres (3D coordinates and radius) are normalized by scaling down to unit length with respect to their minimum and maximum values of the components. Once each lesion is packed by the aforementioned spheres, the following morphological features are extracted.

a) Volume-radius histogram: A histogram in which the radius ranges of internal spheres lie on the x-axis with an arbitrary number of bins and the y-axis is the sum of the spheres volumes with the radius falling into a bin. The sphere packing initially occupies as much volume from the lesion as possible with the biggest possible sphere. Therefore, in benign lesions (with a more regular or round shape), the majority of the lesion space is occupied by a few number of

sizable spheres and the rest by considerably smaller ones. In contrast, in malignant lesions, most of the volume is occupied with medium-sized spheres (Fig. 2).
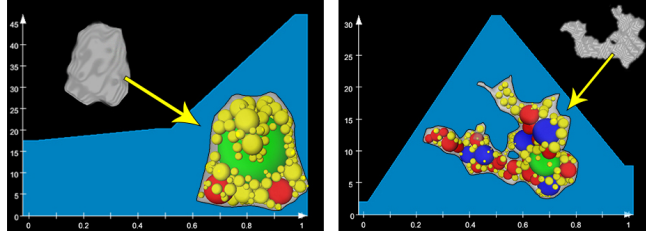
Fig. 2. The volume-radius histogram of two lesions packed with 200 spheres. In benign lesions **(left)** most of their space is filled with sizable spheres; in malignant lesions **(right)**, medium-sized ones occupy most of the internal space.

b) Packing fraction of enclosing sphere: For each lesion, all the internal spheres generated by the sphere packing algorithm were enclosed by a bigger sphere or ball and the occupied fraction of that is calculated as a feature. It is dimensionless and always less in unit range. Several strategies can be applied to define the center point's location of the aforementioned sphere, such as mean centering of coordinates, placing it between the two most distant spheres, in the center of the largest internal sphere, and the center of the smallest enclosing ball [9]. In benign lesions (which often have a regular and round shape) the enclosing sphere is more occupied and has less empty gaps than the malignant ones. This fraction is closer to one for benign and is near zero for malignant lesions.

c) Graph topological features: Graph analysis can assist characterizing the complex structures, leading to a better realization of relations that exist between their components [10]. In this work, it is adapted to characterize the spatial arrangement of the lesion's internal spheres. We constructed the graphs, in which the center points of embedded spheres are considered as nodes, and spatial relationship between them as edges with weights according to their distance. Several structures, including Prim's and Kruskal's minimum spanning trees, relative neighborhood, Gabriel, and β-skeleton graphs were examined to gain the best accuracy (Fig. 3). Finally, the Gabriel graph showed the highest. Furthermore, spatial constraints such as maximum neighbors (K-Max) were employed to form sub-graphs. We used several cluster validity indices, such as graph compactness indices, edge density, structure linearity [11], Dunn's Index, Davies Bouldin index, MinMaxCut, graph's cohesion [12], modularization quality, global silhouette index, Jaccard Coefficient, Folkes, Mallows, Hubert, and Arabie's indices [13] to extract the global and local graph-based geometrical features. The feature vector is formed by the values of all the aforementioned indices.
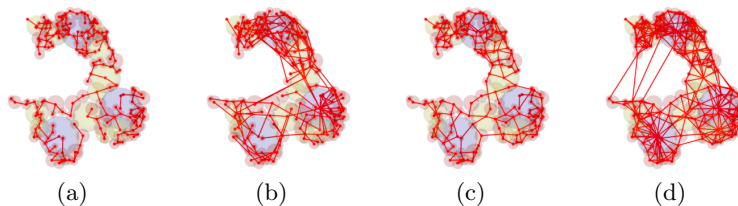
Fig. 3. Kruskal's **(a)** and Prim's **(b)** minimum spanning trees, relative neighborhood **(c)**, and Gabriel **(d)** graph structures obtained by connecting 200 internal spheres.

3D Zernike descriptors Moment-based descriptors have been broadly used for object recognition [8] and shape matching [14] to provide a compact numerical expression of the spatial features. We extracted 3D Zernike descriptors using an extension of spherical-harmonics-based descriptors, presented by Novotni and Klein [15], which captures object coherence in the radial direction.

3 Results and Evaluations

To examine the performance of the proposed features, the first evaluation was conducted without applying any feature selection. We adopted all 106 findings comprising 68 malignant and 38 benign lesions. Each lesion was packed with 4000 spheres. The parameter tuning for the aforementioned features was performed by parameter sweeping of values in a multi-dimensional parameter space and applying the following classification on the feature vectors of each combination to get the best parameter values of the highest accuracy (see Table 1).

Feature extraction module	Parameters	Best value	No. Features
Volume-radius histogram	Number of bins	50	50
Packing fraction of the enclosing ball	Center point's location	Mean centering	1
Graph morphological features	K-Max, Graph type	No. nodes, Gabriel	19
Zernike descriptors	Maximum order	15	72

Table 1. Feature types and their parameter space, plus the optimized values and number of their output features.

For validation of the extracted features, binary classifiers - including Random Forest, Naive Bayes, AdaBoost, and Support Vector Machine (SVM) - were trained with a total of 142 features acquired from the above mentioned methods. For each classifier, a stratified 10-fold cross-validation scheme was applied on the lesions in the data set. The classification power, expressed as AUC is listed in Table 2. The best results were achieved with the RF classifier.

Classifier type	TP Rate		FP Rate		Precision		AUC	
	ben.	mal.	ben.	mal.	ben.	mal.	ben.	mal.
Random Forest	0.78	0.91	0.08	0.21	0.83	0.88	0.90	0.90
Naive Bayes	0.86	0.44	0.55	0.13	0.46	0.85	0.66	0.81
AdaBoost	0.65	0.89	0.10	0.34	0.78	0.82	0.83	0.83
Support Vector Machine	0.68	0.29	0.70	0.31	0.35	0.62	0.48	0.48

Table 2. The TP and FP rates, precision, and AUC values from classification results of different lesion types using four different classifiers (ben. is benign and mal. is malignant). Here the RF classifier outperforms the other three.

3.1 Classification Results with Feature Selection

For the machine learning algorithms, it is important to use feature reduction mechanisms to decrease over-fitting of the training data. Taking advantage of Mean Decrease in Accuracy (MDA) and Mean Decrease GINI (MDG) [16] as variable importance criteria, from a total of 142 features in features set, the top 30 most effective ones were selected for evaluation. Using the RF classifier, MDA ranking showed a higher accuracy than MDG. Among the top features rated by MDA, *volume-radius histogram*, *packed fraction of enclosing ball*, *graph features*, and *Zernike descriptors* features gained the highest order respectively. It should be mentioned that, among those features, only three graph features of *linear structure*, *new compactness index Cp^**, and *Dunn's index* [13] (Eq. 1) appeared on the top 30 MDA features.

$$Dunn(C) = \frac{d(C_i, C_j)}{\text{diam}(C_h)} \qquad , \qquad Cp^* = \frac{\sum_{i=1}^{N-1} \sum_{j=i+1}^{N} \text{sim}(v_i, v_j)}{N(N-1)/2} \qquad (1)$$

Furthermore, applying the Principal Component Analysis (PCA) feature selection was investigated to reduce the dimensionality even more and find the best correlation between the features. However, no improvement was seen in the evaluation results. Table 3 shows the classification results of the RF using 10-FCV before and after applying MDA, MDG, PCA over MDA, and PCA over MDG.

Feature selection	No. features	TP Rate		FP Rate		Precision		Accuracy		AUC	
		ben.	mal.	ben.	mal.	ben.	mal.	ben.	mal.	ben.	mal.
No selection	142	0.789	0.912	0.088	0.211	0.833	0.886	13.2%	86.79%	0.907	0.907
MDG	30	0.816	0.956	0.044	0.184	0.912	0.903	9.43%	90.56%	0.935	0.935
MDA	30	0.816	0.956	0.044	0.184	0.912	0.903	9.43%	90.56%	0.94	0.94
PCA on MDG	5	0.763	0.941	0.059	0.237	0.879	0.877	12.26%	87.73%	0.935	0.935
PCA on MDA	5	0.816	0.926	0.074	0.184	0.861	0.900	11.32%	88.67%	0.936	0.936

Table 3. The classification results of the RF using 10-FCV before and after applying MDA and MDG rankings, plus PCA on them (ben. is benign and mal. is malignant).

4   Conclusion and Discussion

This paper focuses on utilizing the sphere packing (non-overlapping and non -uniform radii) to develop a set of novel morphological features to classify breast non-mass-like lesions. Under the assumption that malignant lesions tend to have irregular shapes and margins compared to benign lesions (which have more regular and round shape), the sphere packing based features can effectively capture the shape differences and thus increase the discrimination accuracy. All the proposed features are translation, rotation, and scaling invariant, since they either are coordinate free features, or because we normalized the data at first.

To our knowledge, this is the first time that such an object representation has been investigated for classifying non-mass lesions in MRI. One advantage of sphere packing is that it can describe volumetric shapes more concisely than a voxel representation or mesh surface. In addition, it allows for deriving additional meta-representations (e.g. proximity graphs and skeletons), which we investigated in this work too. Among many other insights, we discovered that the volume-radius histogram is a particularly efficient shape descriptor to classify non-mass breast lesions into benign and malignant.

To reduce the redundancy of the extracted features, we investigated the application of two feature selection techniques: MDA and PCA to decrease the over-fitting of the data. The classification performance of these features was tested with a data set of 106 non-mass-like lesions collected from 86 patients. Two experiments comparing the performance with and without feature selection were conducted. The classification accuracy, using different classifiers was evaluated. The best AUC value of 0.94 was achieved when using MDA selected features with a RF classifier and 10-FCV scheme. The experiment demonstrated the discriminative power of our proposed features and their potential to increase the diagnostic accuracy of a CAD system. In the future, we will focus on further improving the calculation efficiency of these features and also investigate more features based on the sphere packing.

We acknowledge that there are limitations in our study. Firstly, to the best of our knowledge, there is no validated data set for non-masses publicly available that we can perform a benchmark on and compare the results with others. Therefore, we used aforementioned data set that were labeled meticulously by radiologists, which makes it the best-suited data set for our work. Secondly, we are aware that the evaluation using the 10-FCV method might cause some over-fitting on the data. Nevertheless the 10-FCV is generally even more reliable than other current methods, such as leaveoneout CV and Bootstrap, as it has a lower variance. Reducing the number of features to 30 finals using MDA leads to very low over-fitting and unbiased results at the end.

References

1. S. A. Jansen, A. Shimauchi, L. Zak, X. Fan, G. S. Karczmar, and G. M. Newstead, "The diverse pathology and kinetics of mass, nonmass, and focus enhancement on MR imaging of the breast," *Journal of MRI*, vol. 33, no. 6, pp. 1382–1389, 2011.

2. C. K. Kuhl, S. Schrading, H. B. Bieling, E. Wardelmann, C. C. Leutner, R. Koenig, W. Kuhn, and H. H. Schild, "MRI for diagnosis of pure ductal carcinoma in situ: a prospective observational study," *The Lancet*, vol. 370, no. 9586, pp. 485–492, 2007.

3. S. A. Jansen, X. Fan, G. S. Karczmar, H. Abe, R. A. Schmidt, M. Giger, and G. M. Newstead, "DCEMRI of breast lesions: Is kinetic analysis equally effective for both mass and nonmass-like enhancement?," *Medical physics*, vol. 35, no. 7, pp. 3102–3109, 2008.

4. W. Chen, M. L. Giger, G. M. Newstead, U. Bick, S. A. Jansen, H. Li, and L. Lan, "Computerized assessment of breast lesion malignancy using DCE-MRI: robustness study on two independent clinical datasets from two manufacturers," *Academic radiology*, vol. 17, no. 7, pp. 822–829, 2010.

5. S. Hoffmann, J. D. Shutler, M. Lobbes, B. Burgeth, and A. Meyer-Bäse, "Automated analysis of non-mass-enhancing lesions in breast MRI based on morphological, kinetic, and spatio-temporal moments and joint segmentation-motion compensation technique," *EURASIP Journal on Advances in Signal Processing*, vol. 2013, no. 1, pp. 1–10, 2013.

6. M. Goto, H. Ito, K. Akazawa, T. Kubota, O. Kizu, K. Yamada, and T. Nishimura, "Diagnosis of breast tumors by contrast-enhanced MR imaging: Comparison between the diagnostic performance of dynamic enhancement patterns and morphologic features," *Journal of Magnetic Resonance Imaging*, vol. 25, no. 1, pp. 104–112, 2007.

7. R. Weller and G. Zachmann, "Protosphere: A GPU-assisted prototype guided sphere packing algorithm for arbitrary objects," *ACM SIGGRAPH ASIA*, p. 8, 2010.

8. Z. Chen and S.-K. Sun, "A Zernike moment phase-based descriptor for local image representation and matching," *Image Processing, IEEE Transactions on*, vol. 19, no. 1, pp. 205–219, 2010.

9. B. Gärtner, "Fast and robust smallest enclosing balls," in *European Symposium on Algorithms*, pp. 325–338, Springer, 1999.

10. S. Ali, R. Veltri, J. A. Epstein, C. Christudass, and A. Madabhushi, "Cell cluster graph for prediction of biochemical recurrence in prostate cancer patients from tissue microarrays," in *SPIE Medical Imaging*, pp. 86760H–86760H, International Society for Optics and Photonics, 2013.

11. R. A. Botafogo, E. Rivlin, and B. Shneiderman, "Structural analysis of hypertexts: identifying hierarchies and useful metrics," *ACM Transactions on Information Systems (TOIS)*, vol. 10, no. 2, pp. 142–180, 1992.

12. R. G. Raidou, U. Van Der Heide, C. V. Dinh, G. Ghobadi, J. F. Kallehauge, M. Breeuwer, and A. Vilanova, "Visual analytics for the exploration of tumor tissue characterization," in *Computer Graphics Forum*, vol. 34, pp. 11–20, Wiley Online Library, 2015.

13. F. Boutin and M. Hascoet, "Cluster validity indices for graph partitioning," in *Information Visualisation, 2004. IV 2004. Proceedings. Eighth International Conference on*, pp. 376–381, IEEE, 2004.

14. J. Ricard, D. Coeurjolly, and A. Baskurt, "Generalizations of angular radial transform for 2D and 3D shape retrieval," *Pattern Recognition Letters*, vol. 26, no. 14, pp. 2174–2186, 2005.

15. M. Novotni and R. Klein, "Shape retrieval using 3D Zernike descriptors," *Computer-Aided Design*, vol. 36, no. 11, pp. 1047–1062, 2004.

16. M. L. Calle and V. Urrea, "Letter to the editor: stability of random forest importance measures," *Briefings in bioinformatics*, p. bbq011, 2010.